$K_2FeFe(CN)_6$, 15362-86-4; $Li_2FeFe(CN)_6$, 92937-93-4; $Na_2FeFe(CN)_6$, 92937-94-5; $FeFe(CN)_6$, 14433-93-3; $K_3Fe(CN)_6$, 13746-66-2; $Na_3Fe(CN)_6$, 14217-21-1; $K_4Fe(CN)_6$, 13943-58-3; $Na_4Fe(CN)_6$, 13601-19-9; $Li_4Fe(CN)_6$, 13601-18-8; $NaFeFe(CN)_6$, 51041-36-2; $LiFeFe(CN)_6$, 51041-35-1; $LiClO_4$, 7791-03-9; $KClO_4$, 7778-74-7; $NaClO_4$, 7601-89-0; KPF_6, 17084-13-8; KNO_3, 7757-79-1; $NaNO_3$, 7631-99-4; $LiNO_3$, 7790-69-4; C_2H_6, 74-84-0; Li, 7439-93-2; Na, 7440-23-5; K, 7440-09-7; graphite, 7782-42-5.

Contribution from the P. M. Gross Chemical Laboratory, Department of Chemistry, Duke University, Durham, North Carolina 27706

Kinetics, Mechanism, and Thermodynamics of Aqueous Iron(III) Chelation and Dissociation: Influence of Carbon and Nitrogen Substituents in Hydroxamic Acid Ligands

CHRISTINA POTH BRINK and ALVIN L. CRUMBLISS*

Received January 25, 1984

Thermodynamic and kinetic studies were performed to investigate the complexation of aqueous high-spin iron(III) by 12 bidentate hydroxamic acids, $R_1C(O)N(OH)R_2$, (R_1 = CH_3, C_6H_5, 4-$NO_2C_6H_4$, 4-$CH_3C_6H_4$, 4-$CH_3OC_6H_4$; R_2 = CH_3, C_6H_5, 4-$CH_3C_6H_4$, 4-ClC_6H_4, 4-IC_6H_4, 3-IC_6H_4, 4-NCC_6H_4, 3-NCC_6H_4, 4-$CH_3C(O)C_6H_4$), in acid medium. Both complex formation and dissociation (aquation) reactions were investigated by stopped-flow relaxation methods over a range of $[H^+]$ and temperatures. A two-parallel-path mechanism without proton ambiguity is established for the reaction of $Fe(H_2O)_6^{3+}$ and $Fe(H_2O)_5OH^{2+}$ with $R_1C(O)N(OH)R_2$ to form $Fe(H_2O)_4(R_1C(O)N(O)R_2)^{2+}$. Equilibrium quotients, ΔH° and ΔS° values, rate constants, and $\Delta H^\ddagger$ and $\Delta S^\ddagger$ values for both reaction paths in the forward and reverse directions are reported. $\Delta H^\ddagger$ and $\Delta S^\ddagger$ values are found to be linearly related and compensating. On the basis of an analysis of the equilibrium quotients, rate constants, and activation parameters for the reaction in both directions, an associative interchange (I_a) mechanism is proposed for hydroxamic acid ligand substitution at $Fe(H_2O)_6^{3+}$. Similar trends for these parameters are observed for the reaction at $Fe(H_2O)_5OH^{2+}$, suggesting an associative interchange character for this reaction path also. However, coordinated water dissociation appears to be dominant, and some associative character for this path may be the result of H-bonding interactions between the undissociated hydroxamic acid and coordinated -OH. Electron-donating and -withdrawing R_1 and R_2 substituents were selected in order to determine the relative influence of the C and N substituent on the hydroxamic acid and to determine the optimum hydroxamic acid structure for kinetic and thermodynamic stability of the iron(III) chelate. Kinetic and thermodynamic chelate stabilization are enhanced by increasing electron density on the carbonyl oxygen atom, which is promoted by electron donors in the R_1 position and delocalization of the N atom lone pair of electrons into the C-N bond. The influence of the R_2 substituent appears to be dominant with an electron-releasing alkyl group as the preferred R_2 substituent for kinetic and thermodynamic stability. The optimum hydroxamic acid ligand for kinetic and thermodynamic stability of the iron(III) chelate was found to be 4-$CH_3OC_6H_4C(O)N(OH)CH_3$.

Introduction

Hydroxamic acids have broad application as corrosion inhibitors, antifungal agents, food additives, flotation reagents in extractive metallurgy, pharmaceutical, and analytical reagents.[1] Several of these applications depend on the strong metal-complexing ability of the hydroxamates. Of particular interest and relevance to this report is the high affinity of the hydroxamate group for iron(III). Siderophores, which are microbially generated chelators produced to increase the bioavailability of iron to these organisms, are known to contain hydroxamic acid functional groups.[2,3] Synthetic and naturally occurring hydroxamic acids have been investigated for use as therapeutic agents for iron removal from transfusion-induced iron-overloaded patients.[4,5] For a number of reasons it is of interest to obtain an understanding of the kinetic and thermodynamic contribution to iron(III) complex stability with hydroxamic acid ligands, as well as the mechanism for iron(III) chelation and release (reaction 1). Previous work in our

$$Fe(H_2O)_6^{3+} + R_1C(O)N(OH)R_2 \underset{}{\overset{H_2O}{\rightleftharpoons}} Fe(H_2O)_4(R_1C(O)N(O)R_2)^{2+} + H_{aq}^+ + 2H_2O \quad (1)$$

laboratory has dealt with the thermodynamics, kinetics, and mechanism of reaction 1 with a series of synthetic hydroxamic acids where R_1 = CH_3 and C_6H_5 and R_2 = CH_3, C_6H_5, and H.[6] We have applied the mechanistic model developed for reaction 1 to iron(III) dissociation from the siderophore ferrioxamine B[7,8] in acid solution and at conditions where the dissociation reaction is catalyzed by synthetic hydroxamic acids.[9]

In this report we describe a systematic investigation of the electronic influence of the substituent on the C (R_1 group) and the N (R_2 group) atoms of the hydroxamate moiety on the thermodynamics, kinetics, and mechanism of reaction 1. Two series of synthetic hydroxamic acids were used: the substituted *N*-methylbenzohydroxamic acids (I) (referred to as the R_1 series) and the substituted *N*-phenylacetohydroxamic acids (II) (referred to as the R_2 series). Complex formation constants, kinetics of complex formation and dissociation, and associated

(1) (a) Kehl, H., Ed. "Chemistry and Biology of Hydroxamic Acids"; Karger: New York, 1982. (b) Bauer, L.; Exner, O. *Angew. Chem., Int. Ed. Engl.* **1974**, *13*, 376. (c) Agrawal, Y. K. *Russ. Chem. Rev.* (*Engl. Transl.*) **1979**, *48*, 948. (d) Agrawal, Y. K.; Roshania, R. D. *Bull. Soc. Chim. Belg.* **1980**, *89*, 159. (e) Agrawal, Y. K. *Rev. Anal. Chem.* **1980**, *5*, 3. (f) Chatterjee, B. *Coord. Chem. Rev.* **1978**, *26*, 281.
(2) Neilands, J. B. *Annu. Rev. Biochem.* **1981**, *50*, 715.
(3) Neilands, J. B. *Adv. Inorg. Biochem.* **1983**, *5*, Chapter 6.
(4) Martell, A. E., Anderson, W. F., Badman, D. G., Eds. "Development of Iron Chelators for Clinical Use"; Elsevier, New York, 1981.
(5) Brown, D. A.; Chidambaram, M. B. In "Metal Ions in Biological Systems"; Sigel, H., Ed.; Marcel Dekker: New York, 1982; Vol. 14, Chapter 5.
(6) Monzyk, B.; Crumbliss, A. L. *J. Am. Chem. Soc.* **1979**, *101*, 6203.
(7) Monzyk, B.; Crumbliss, A. L. *Inorg. Chim. Acta* **1981**, *55*, L5.
(8) Monzyk, B.; Crumbliss, A. L. *J. Am. Chem. Soc.* **1982**, *104*, 4921.
(9) Monzyk, B.; Crumbliss, A. L. *J. Inorg. Biochem.* **1983**, *19*, 19.

0020-1669/84/1323-4708$01.50/0

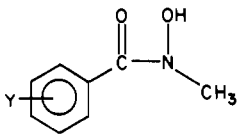

I: Y = H, 4-NO_2, 4-CH_3, 4-CH_3O

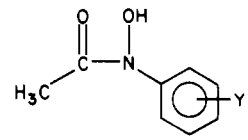

II: Y = H, 4-CH_3, 4-Cl, 4-I, 3-I, 4-CN, 3-CN, 4-$C(O)CH_3$

temperature dependencies for this series of 12 related hydroxamic acids are reported. The R_1 and R_2 series are designed in order to determine in both kinetic and thermodynamic terms (1) what the optimum R_1 substituent is for complex stability, (2) what the optimum R_2 substituent is for complex stability, and (3) which group, R_1 or R_2, has the dominant influence.

Complex *formation* kinetic data have appeared in the literature for mono(hydroxamic acid)[10-13] and deferriferrioxamine B[14-17] reactions with Fe_{aq}^{3+}, as well as iron-exchange reactions with ferrioxamine B[18] and tris(acetohydroxamato)iron(III).[19,20] This report, along with our previous report,[6] represents a systematic investigation of the influence of structural changes in a homologous series of ligands on the thermodynamics, kinetics, and mechanism of Fe_{aq}^{3+} complex *formation and dissociation*. The inclusion of dissociation kinetic data along with activation parameters for the series also allows us to further probe the general question of the intimate mechanism for ligand substitution at high-spin aqueous iron(III).

Experimental Section

Materials. Iron(III) perchlorate (G. F. Smith) was recrystallized twice from dilute perchloric acid before use. Sodium perchlorate was prepared by neutralization of Na_2CO_3 (Fisher, ACS Certified) by $HClO_4$ (Mallinckrodt) and was recrystallized from water prior to use. All solutions were prepared with water distilled once from acidic $K_2Cr_2O_7$ and then slowly from basic $KMnO_4$ in an all-glass apparatus with Teflon sleeves and stopcocks. All hydroxamic acids were prepared and characterized as described previously.[21,22] Purity was checked by C, H, and N analyses (M-H-W Laboratories, Phoenix, AZ) and iron(III) complex extinction coefficients.

Methods. Preparation of Solutions. Care was taken in the preparation and manipulation of iron(III) solutions in order to prevent extensive hydrolysis that would complicate equilibrium and kinetic measurements.[23] The results of previous studies were used to determine the extent and influence of iron(III) hydrolysis at various acidities, iron(III) concentrations, temperatures, and ionic strengths.[24-26] All of our studies were performed at conditions such that the only aqueous iron(III) species present to a significant extent were $Fe(H_2O)_6^{3+}$ and $Fe(H_2O)_5OH^{2+}$. The maximum concentration of the latter was never more than 1% of the total amount of iron(III) present.

Stock aqueous iron(III) solutions were prepared with [Fe(III)] ~ 0.1 M and $[HClO_4]$ ~ 0.1 M. (Here, [Fe(III)] represents the total uncomplexed iron(III) concentration, i.e., $[Fe(III)] = [Fe(H_2O)_6^{3+}] + [Fe(H_2O)_5OH^{2+}]$). The stock iron(III) solutions were standardized with a standard solution of triply recrystallized $K_2Cr_2O_7$ after reduction with stannous ion according to normal procedures.[27] The acidity of the stock iron(III) solution ($[HClO_4]$ ~ 0.1 M) was determined by passing an aliquot through a Dowex 50W-X8 20–50-mesh cation-exchange resin in the acid form. The liberated H^+ was titrated with standardized NaOH to the phenolphthalein end point, and corrections were made for the iron(III) present. All determinations were made in triplicate.

Stock $NaClO_4$ solutions, used to maintain constant ionic strength, were standardized by passing an aliquot through a Dowex 50W-X8 20–50-mesh cation-exchange column in the acid form and titrating the liberated H^+ to the phenolphthalein end point.

Reagent mono(hydroxamato)iron(III) ($Fe(H_2O)_4(R_1C(O)N(O)R_2)^{2+}$) complex solutions (~$10^{-3}$ M) were carefully prepared (by weight) to contain equimolar amounts of iron(III) and ligand at $[H^+] = 10^{-2}$ M. The appropriate weight of the stock iron(III) solution was calculated from the solution density. Solutions were prepared by dilution of the stock iron(III) solution with aqueous $HClO_4/NaClO_4$ (adding acid first). Addition of the solid preweighed hydroxamic acid followed. The final volume was adjusted with 2.0 M $NaClO_4$. After dilution, 2–24 h was allowed for the solutions to reach equilibrium. This is to ensure equilibrium of any hydrolysis products in the concentrated iron(III) stock solution. Solutions were used immediately after the period allowed for equilibration, with a series of kinetic runs never lasting longer than 60 h. These solutions are stable at room temperature up to 4 days at $[H^+] = 10^{-2}$ M.[6] When necessary, reagent solutions were stored overnight in a refrigerator.

The absorption maxima, λ_{max}, and molar absorptivities, ϵ, for the mono(hydroxamato)iron(III) complexes were determined from mole ratio experiments at the conditions of excess iron(III) ([Fe(III)]/[HA] up to 190/1), 0.1 M $HClO_4$, and 2.0 M ionic strength ($NaClO_4$), on a Beckman Acta III recording double-beam spectrophotometer equipped with a water-jacketed cell holder maintained at 25 °C. UV data: $Fe(CH_3C(O)N(O)\text{-}4\text{-}C_6H_4C(O)CH_3)(H_2O)_4^{2+}$, 505 nm ($\epsilon$ = 1269 M^{-1} cm^{-1}); $Fe(CH_3C(O)N(O)\text{-}4\text{-}C_6H_4CN)(H_2O)_4^{2+}$, 500 (1250); $Fe(CH_3C(O)N(O)\text{-}3\text{-}C_6H_4CN)(H_2O)_4^{2+}$, 500 (1251); $Fe(CH_3C(O)N(O)\text{-}4\text{-}C_6H_4I)(H_2O)_4^{2+}$, 505 (1250); $Fe(CH_3C(O)N(O)\text{-}3\text{-}C_6H_4I)(H_2O)_4^{2+}$, 504 (1502); $Fe(CH_3C(O)N(O)\text{-}4\text{-}C_6H_4Cl)(H_2O)_4^{2+}$, 504 (1241); $Fe(CH_3C(O)N(O)\text{-}4\text{-}C_6H_4CH_3)(H_2O)_4^{2+}$, 508 (1664); $Fe(4\text{-}NO_2C_6H_4C(O)N(O)CH_3)(H_2O)_4^{2+}$, 499 (1424); $Fe(4\text{-}CH_3C_6H_4C(O)N(O)CH_3)(H_2O)_4^{2+}$, 514 (1391); $Fe(4\text{-}CH_3OC_6H_4C(O)N(O)CH_3)(H_2O)_4^{2+}$, 521 (1403); $Fe(4\text{-}CH_3OC_6H_4C(O)N(O)H)(H_2O)_4^{2+}$, 540 (1586).

Equilibrium Measurements. The determination of hydroxamic acid ligand pK_a values as a function of temperature has been described.[21,22] Data for mono(hydroxamato)iron(III) complex formation constant calculations were obtained in two ways. In one method, static absorbance measurements were made at 25 °C at a fixed $[H^+]$ (0.1 M) and a variable [Fe(III)]/[HA] ratio (0.3–190), which corresponds to between 5 and 100% complexation. The measurements were made in the region from 400 to 700 nm for each complex on a Beckman Acta III spectrophotometer equipped with a water-jacketed cell holder. In the second method, infinite time–absorbance readings were taken from kinetic experiments where the [Fe(III)]/[HA] ratio was fixed ($[Fe(III)] = [HA] \sim 10^{-3}$ M) and the $[H^+]$ varied over the range from 0.025 to 1.00 M. These data were collected over the temperature range from 20 to 45 °C and were used to compute $\Delta H_f°$ and $\Delta S_f°$ values for complex formation.

Kinetic Measurements. An Aminco stopped-flow apparatus employing a Beckman DU monochromator was used for all of the kinetic measurements. Experiments utilized a digital data acquisition system developed by interfacing the Aminco instrument to a Cybertech LP-12 12-bit microcomputer. Data were then fed to a DEC Model PDP8/f and later to an Apple II minicomputer for data analysis.[6] This process yielded from 50 to 60 data points per each observed rate constant. Kinetic data were collected at the λ_{max} value for each of the mono(hydroxamato)iron(III) complexes.

Temperature control was maintained with the use of a Forma Scientific Model 2095 constant-temperature bath over the range of

(10) Kazmi, S. A.; McArdle, J. V. *J. Inorg. Nucl. Chem.* **1981**, *43*, 3031.
(11) Birus, M.; Kujundzic, N.; Pribanic, M. *Inorg. Chim. Acta* **1980**, *55*, 65.
(12) Fujundzic, N.; Pribanic, M. *J. Inorg. Nucl. Chem.* **1978**, *40*, 789.
(13) Junahashi, S.; Ishihara, K.; Tanaka, M. *Inorg. Chem.* **1983**, *22*, 2070.
(14) Kazmi, S. A.; McArdle, J. V. *J. Inorg. Biochem.* **1981**, *15*, 153.
(15) Birus, M.; Bradic, Z.; Kujundzic, N.; Pribanic, M. *Inorg. Chim. Acta* **1981**, *56*, L43.
(16) Birus, M.; Bradic, Z.; Kujundzic, N.; Pribanic, M. *Inorg. Chim. Acta* **1983**, *78*, 87.
(17) Birus, M.; Bradic, Z.; Kujundzic, N.; Pribanic, M. *Croat. Chem. Acta* **1983**, *56*, 61.
(18) Tufano, T. P.; Raymond, K. N. *J. Am. Chem. Soc.* **1981**, *103*, 6617.
(19) (a) Brown, D. A.; Chidambaram, M. V.; Clarke, J. J.; McAleese, D. M. *Bioinorg. Chem.* **1978**, *9*, 255. (b) Brown, D. A.; Chidambaram, M. V.; Glennon, J. D. *Inorg. Chem.* **1980**, *19*, 3260.
(20) Cavart, R. E.; Kojima, N.; Bates, G. W. *J. Biol. Chem.* **1982**, *257*, 7560.
(21) Brink, C. P.; Crumbliss, A. L. *J. Org. Chem.* **1982**, *47*, 1171.
(22) Brink, C. P.; Fish, L. L.; Crumbliss, A. L. *J. Org. Chem.*, in press.
(23) Siddall, T. H., III; Vosburgh, W. C. *J. Am. Chem. Soc.* **1951**, *73*, 4270.
(24) Milburn, R. M. *J. Am. Chem. Soc.* **1957**, *79*, 537.
(25) Wendt, H. *Z. Elektrochem.* **1962**, *66*, 235.
(26) Sommer, B. A.; Margerum, D. W. *Inorg. Chem.* **1970**, *9*, 2517.
(27) Skoog, D. A.; West, D. M. "Fundamentals of Analytical Chemistry", 2nd ed.; Holt, Rinehart and Winston: New York, 1963; p 437.

Table I. Thermodynamic Data for Mono(hydroxamato)iron(III) Complex Formation

	$R_1C(O)N(OH)R_2$			reaction 7			reaction 9		
no.	R_1	R_2	pK_a[a] (25 °C)	$10^{-2}Q_f$,[b] (25 °C)	ΔH_f°,[c] kcal/mol	ΔS_f°,[c] cal/(K mol)	$10^{-10}Q_f$, (25 °C),[d] M^{-1}	$\Delta H_f^{\circ\prime}$,[e] kcal/mol	$\Delta S_f^{\circ\prime}$,[e] cal/(K mol)
1	4-$CH_3OC_6H_4$	CH_3	8.67	15.46 (0.90)	2.9 (0.2)	23 (1)	72.3	+1.7 (0.3)	59 (2)
2	4-$CH_3C_6H_4$	CH_3	8.50	14.41 (0.81)	0.5 (0.03)	15 (0.1)	45.7	−1.1 (0.2)	48 (1)
3	C_6H_5	CH_3	8.28[f]	5.49 (0.22)[g]	1.0 (0.2)[g]	17 (1)[g]	10.4[f]	−1.2 (0.4)[f]	48 (2)[f]
4	4-$NO_2C_6H_4$	CH_3	7.94	2.99 (0.18)	0.9 (0.1)	14 (0.4)	2.60	−0.2 (1.6)	47 (1)
5	CH_3	4-$C_6H_4CH_3$	8.81	2.94 (0.10)	3.5 (1.5)	23 (5)	19.0	−4.1 (2.4)	38 (8)
6	CH_3	C_6H_5	8.42	2.25 (0.09)[g]	1.3 (0.1)	16 (10)	4.93	−9.6 (1.1)	18 (4)
7	CH_3	4-C_6H_4I	8.29	1.85 (0.03)	4.8 (0.7)	26 (2)	3.61	−0.9 (1.3)	45 (4)
8	CH_3	4-C_6H_4Cl	8.37	1.21 (0.11)	3.8 (2.0)	23 (7)	2.84	−2.5 (3.6)	40 (12)
9	CH_3	3-C_6H_4I	8.31	1.66 (0.10)	4.9 (0.6)	26 (2)	3.39	−1.4 (1.2)	43 (4)
10	CH_3	3-C_6H_4CN	8.26	0.92 (0.04)	3.6 (1.1)	20 (4)	1.67	−5.2 (1.6)	28 (6)
11	CH_3	4-$C_6H_4C(O)CH_3$	8.34	1.04 (0.04)	4.0 (3.0)	22 (8)	2.28	−3.8 (3.5)	34 (10)
12	CH_3	4-C_6H_4CN	8.25	0.54 (0.06)	6.8 (1.3)	30 (4)	0.96	−0.2 (2.0)	44 (6)
13	4-$CH_3OC_6H_4$	H[h]	8.76	2.49 (0.01)	3.1 (0.2)	20 (1)	14.3	−2.5 (0.5)	41 (2)

[a] From ref 21 and 22. [b] Formation quotients for reaction 7 calculated according to eq 2. Values listed represent an average of four to eight determinations at different [Fe(III)]/[HA] ratios (I = 2.00 ($NaClO_4$/$HClO_4$)). [c] ΔH_f° and ΔS_f° for reaction 7 calculated from Q_f data obtained from eq 3 over the temperature range from 20 to 45 °C. Values listed represent an average of 9-20 determinations at each of five temperatures (I = 2.00 ($NaClO_4$/$HClO_4$)). [d] Formation quotient for the nonexperimentally accessible reaction 9 calculated according to $Q_f' = Q_f/K_a$ at 25 °C. [e] $\Delta H_f^{\circ\prime}$ and $\Delta S_f^{\circ\prime}$ for nonexperimentally accessible reaction 9 calculated from ΔH_f° and ΔS_f° for reaction 7 and ΔH_a° and ΔS_a° for reaction 8 obtained from ref 21 and 22. [f] Redetermination of value found in ref 40 and recalculation of values in ref 6; see ref 22. [g] Reference 6. [h] Reference 39.

20–45 °C. Temperature control precision was 0.1 °C over this range. The temperature at which kinetic experiments were performed was obtained by measuring the temperature of the circulation liquid immediately after it exited from the syringe block of the stopped-flow apparatus.

Relaxation kinetics were studied by flowing together a mono(hydroxamato)iron(III) complex solution (typically [Fe(III)] = [HA] = 10^{-3} M, [$HClO_4$] = 0.01 M, I = 2.0 M ($NaClO_4$)) with a solution of increased acid concentration (typically [$HClO_4$] = 0.05–2.0 M, I = 2.0 M ($NaClO_4$/$HClO_4$)). Each experimental rate constant reported in the Results is based on 50–60 data points from each of three to five separate stopped-flow injections.

Results

Complex Stoichiometry. Spectral data for all hydroxamic acids investigated, collected over the wavelength range from 400 to 700 nm, show a single λ_{max} and ϵ_{max} for the [Fe(III)]/[HA] ratios studied up to 190/1. The shape and position of this absorption band remain constant and its absorptivity reaches a maximum at [Fe(III)]/[HA] ~ 40/1 for [H^+] = 0.1 M and 25 °C. This is consistent with the formation of a single absorbing species, a mono(hydroxamato)iron(III) complex, in solution and is identical with previous results obtained in this laboratory[6] where matrix methods[28] were also used to establish a 1/1 hydroxamic acid/iron(III) stoichiometry. Additional characterization of the complex stoichiometry in the case of the Fe(III)/$CH_3C(O)N(OH)$-4-$C_6H_4CH_3$ system was obtained by the method of continuous variations.[29] The absorbance vs. mole fraction plot shows a maximum at 0.5 (±5%) mole fraction, indicating that the absorbing species contains hydroxamic acid and iron(III) in a 1/1 ratio.

Acid dissociation constants, and their associated temperature dependencies, were determined for all 12 hydroxamic acids[21,22] with conditions identical with those in the complexation studies. The pK_a values fall in the range from 8 to 9 so the hydroxamic acids are undissociated at the conditions of our complexation studies. The reaction of interest in our investigation is the formation of the mono(hydroxamato)iron(III) complex from hexaaquoiron(III) and free hydroxamic acid ligand according to eq 1. Since this investigation was carried out at conditions such that the bis and tris complexes were not formed and therefore $Fe(H_2O)_4(R_1C(O)N(O)R_2)^{2+}$ was the only absorbing species in solution, the equilibrium quotient, Q_f, for reaction 1 was calculated in the usual way from the equation

$$Q_f = [FeA^{2+}][H^+]/[Fe^{3+}][HA] \quad (2)$$

(For clarity, HA and A^- represent the hydroxamic acid and the hydroxamate anion, respectively; coordinated H_2O is omitted.) The various quantities in eq 2 were determined as follows: $[FeA^{2+}] = A_e/l\epsilon$ at the λ_{max} value for each complex; $[Fe^{3+}] = [Fe(III)]_{tot} - [FeA^{2+}]$; $[HA] = [HA]_{tot} - [FeA^{2+}]$. The [$H^+$] was in large excess and was calculated from the known acidities of the reagent solutions.

Equilibrium quotients, Q_f, for reaction 1 were calculated with eq 2 and data obtained at conditions where complex formation was between 15 and 85% complete. The results of these experiments performed at 25.0 °C are listed in Table I. Values for Q_f' defined as the formation quotient for reaction with the hydroxamate anion may be calculated from Q_f values and hydroxamic acid acidity constants.[21,22] These values are also listed in Table I.

Enthalpy and entropy changes associated with complex formation were calculated from equilibrium $[Fe(H_2O)_4(R_1C(O)N(O)R_2)^{2+}]$ determined over a 25 °C temperature range. These data were obtained from kinetic experiments (described below and in the Experimental Section). The experimental conditions allowed Q_f to be calculated at each temperature according to the equation

$$C_{tot}/A_e = ([H^+]/A_e)^{1/2}/(\epsilon Q_f)^{1/2} + 1/\epsilon \quad (3)$$

where $C_{tot} = [Fe(III)]_{tot} = [HA]_{tot}$ and A_e = total absorbance at equilibrium. Q_f was obtained from the slope of a plot of C_{tot}/A_e vs. $([H+]/A_e)^{1/2}$, with a value of ϵ obtained from mole ratio plots described above.[30] The ΔH_f° and ΔS_f° values for reaction 1 obtained from eq 3 are listed in Table I. Also listed in Table I are $\Delta H_f^{\circ\prime}$ and $\Delta S_f^{\circ\prime}$ values for the reaction of $Fe(H_2O)_6^{3+}$ with the hydroxamate anion, which were calcualted from ΔH_f° and ΔS_f° for reaction 1 and ΔH_a and ΔS_a for acid dissociation.[21,22]

Kinetics. Relaxation kinetic studies were carried out by rapidly increasing the [H^+] of an iron(III)–hydroxamic acid

(28) Coleman, J. S.; Varga, L. P.; Mastin, S. H. *Inorg. Chem.* **1970**, *9*, 1015.
(29) Vosburgh, W. C.; Cooper, G. R. *J. Am. Chem. Soc.* **1941**, *63*, 437.
(30) Values of ϵ were not determined from the intercepts of the plots according to eq 3 as they are inherently of low precision: Rose, N. J.; Drago, R. S. *J. Am. Chem. Soc.* **1959**, *81*, 6138.

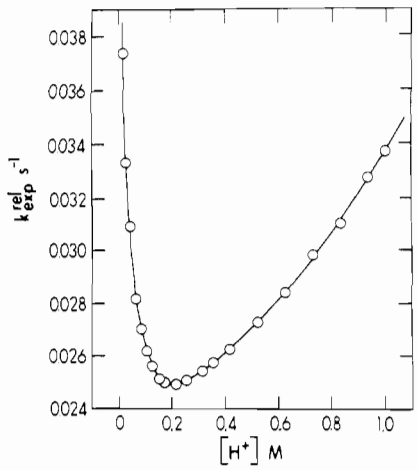

Figure 1. Plot of k_{exptl}^{rel} vs. $[H^+]$ for the $Fe(H_2O)_4(CH_3C(O)N(O)\text{-}4\text{-}C_6H_4I)^{2+}$ system at 25 °C. Each data point represents three to five independent determinations of k_{exptl}^{rel}; standard deviations are smaller than the data point size. The solid line represents a least-squares fit of the data to eq 4 and 11. See Table V for data.[31] Conditions: $[Fe(III)] = [HA] = 4.99 \times 10^{-4}$ M; $I = 2.00$ M ($NaClO_4/HClO_4$).

complex solution (where $[Fe(III)]_{tot} = [HA]_{tot}$) from 0.01 to 0.025–1.00 M. This results in the measurement of a first-order rate constant, k_{exptl}^{rel}, which corresponds to the relaxation to a new equilibrium position. Tables II–XII[31] are a compilation of first-order relaxation rate constants, k_{exptl}^{rel}, obtained as a function of $[H^+]$ at various temperatures from 20 to 45 °C. Figure 1 is a representative plot of these data at 25 °C for $Fe(H_2O)_4(CH_3C(O)N(O)\text{-}4\text{-}C_6H_4I)^{2+}$. The solid line represents a least-squares fit of the three-parameter equation (4) to the experimental data. A good fit of eq 4 to the relaxation rate constants was obtained for all 12 iron(III)/hydroxamate systems over the temperature range investigated.

$$k_{exptl}^{rel} = a + b/[H^+] + c[H^+] \quad (4)$$

Taking into consideration the hydrolysis of $Fe(H_2O)_6^{3+}$ and the hydroxamic acid dissociation equilibrium, the simplest mechanism to consider for reaction 1 is presented in Scheme I. It can be shown that when the reaction mechanism shown

Scheme I

path 2: $Fe(H_2O)_5OH^{2+} + HA \overset{Q_f''}{\rightleftharpoons}$

$$\begin{array}{c} +H^+ \downarrow\uparrow -H^+ \end{array} \qquad Fe(H_2O)_4A^{2+} + 2H_2O \quad k_2/k_{-2} \quad (5)$$

$$K_h \quad (6)$$

path 1: $Fe(H_2O)_6^{3+} + HA \overset{Q_f}{\rightleftharpoons} Fe(H_2O)_4A^{2+} +$

$$-H^+ \downarrow\uparrow +H^+ \qquad H_{aq}^{+} + 2H_2O \quad k_1/k_{-1} \quad (7)$$

$$K_a \quad (8)$$

path 3: $Fe(H_2O)_6^{3+} + A^- \overset{Q_f'}{\rightleftharpoons} Fe(H_2O)_4A^{2+} + 2H_2O \quad k_3/k_{-3} \quad (9)$

in Scheme I is treated as a relaxation process at the conditions where $[Fe(III)]_{tot} = [HA]_{tot} = C_{tot}$, then the equation (10) may

$$k_{exptl}^{rel} = 2k_1(C_{tot} - [FeA^{2+}]_e) + k_{-2} + k_{-3} + ((2k_2K_h + 2k_3K_a)(C_{tot} - [FeA^{2+}]_e))/[H^+] + k_{-1}[H^+] \quad (10)$$

be derived for the relaxation rate constant k_{exptl}^{rel}.[6] The equilibrium complex concentration, $[FeA^{2+}]_e$, was determined from A_e/ϵ. Path 3 (reaction 9) may be eliminated from consideration over the $[H^+]$ range investigated due to the low acidity constants ($pK_a = 8$–9, reaction 8) of the hydroxamic acids.[21,22] Furthermore, if one assumes that the $[H^+]^{-1}$ dependence of k_{exptl}^{rel} arises from path 3, the forward rate constant k_3 is calculated to be on the order of 10^9 M^{-1} s^{-1}. This is much too high a value for substitution at an aqueous iron(III) center. For these reasons path 3 was assumed to make only a negligible contribution to the total rate of complex formation at our conditions. Furthermore, at our conditions the term $2k_1(C_{tot} - [FeA^{2+}]_e)$ is small compared to all other terms. These observations allow for a simplification of eq 10 as

$$k_{exptl}^{rel} = k_{-2} + (2k_2K_h(C_{tot} - [FeA^{2+}]_e))/[H^+] + k_{-1}[H^+] \quad (11)$$

This equation is of the same form as the empirical eq 4, where $a = k_{-2}$, $b = 2k_2K_h(C_{tot} - [FeA^{2+}]_e)$, and $c = k_{-1}$. Values for the rate constants k_2, k_{-2}, and k_{-1} calculated at each temperature were obtained from a least-squares fit of eq 11, rearranged as shown in eq 12, to the data. A total of 1100 k_{exptl}^{rel}

$$k_{exptl}^{rel}[H^+] = 2k_2K_h(C_{tot} - [FeA^{2+}]_e) + k_{-2}[H^+] + k_{-1}[H^+]^2 \quad (12)$$

values (each representing an average of four determinations) were obtained for all 12 mono(hydroxamato)iron(III) complexes at various $[H^+]$ and temperatures from 20 to 45 °C (see Tables II–XII[31]). Each microscopic rate constant was determined from 15–20 k_{exptl}^{rel} values at a given temperature. Values for k_2, k_{-2}, and k_{-1} obtained in this way are listed in Table XIII. The values for k_1 (see Table XIII) were calculated from Q_f (determined from mole ratio experiments (Table I)) and k_{-1} (Table XIII) according to the relationship $Q_f = k_1/k_{-1}$. Activation parameters ($\Delta H^{\ddagger}$, $\Delta S^{\ddagger}$; Table XIII) were obtained from relaxation experiments by plotting each of the derived rate constants (k_{-1}, k_{-2}, k_2) as $\ln (k/T)$ vs. $1/T$. Activation parameters listed in Tables XIII for complex formation via path 1 ($\Delta H^{\ddagger}_1$, $\Delta S^{\ddagger}_1$) were calculated from the corresponding aquation activation ($\Delta H^{\ddagger}_{-1}$, $\Delta S^{\ddagger}_{-1}$) and thermodynamic parameters ($\Delta H_f°$, $\Delta S_f°$).

Discussion

Equilibrium Studies. Table I is a collection of the thermodynamic parameters for mono(hydroxamato)iron(III) complex stability. Although path 3 in Scheme I was eliminated as an experimentally accessible path at our conditions, the availability of ligand pK_a data[21,22] allows the equilibrium quotient, Q_f', for the reaction shown in eq 9 to be calculated. These large Q_f' values (10^{10}–10^{12} M^{-1}; Table I) place the bidentate hydroxamate group among the most stable chelators for binding to Fe_{aq}^{3+}.[32]

The enthalpy ($\Delta H_f°$, $\Delta H_f°'$) and entropy ($\Delta S_f°$, $\Delta S_f°'$) values were computed from the temperature dependence of Q_f and K_a.[21,22] These data are listed in Table I and show that in all but one case complexation of $Fe(H_2O)_6^{3+}$ with the hydroxamate anion is exothermic and in all cases is accompanied by a large positive entropy change. This is consistent with a strong chelate effect. The reaction of $Fe(H_2O)_6^{3+}$ with the undissociated ligand is endothermic because reaction 7 is a composite of reactions 8 and 9 (K_a and Q_f'). The large, positive entropy changes ($\Delta S_f°$ and $\Delta S_f°'$) shown in Table I are most likely due to solvation changes as well as to the chelate effect (see below).

Equilibrium Studies: R_2 Series. The electronic influence of the R_2 functional group on the thermodynamics of iron(III) complex formation has been investigated on a wide range of hydroxamic acids, II, where $R_1 = CH_3$ and $R_2 = C_6H_4Y$ (Y = H, 4-CH_3, 4-Cl, 4-I, 3-I, 4-CN, 3-CN, 4-$C(O)CH_3$). The

(31) See paragraph at end of paper regarding supplementary material.

(32) For a recent compilation of metal–ligand binding constants see: Martell, A. E.; Smith, R. M. "Critical Stability Constants"; Plenum Press: New York, 1977.

Table XIII. Kinetic Parameters Corresponding to Scheme I[a]

no.	$R_1C(O)N(OH)R_2$ R_1	R_2	k_{exptl}^{rel} ($25\,^{\circ}C$), $M^{-1}\,s^{-1}$	$\Delta H^{\ddagger}_{1}$, kcal/mol	$\Delta S^{\ddagger}_{1}$, cal/(K mol)	$10^{-3}k_2$ ($25\,^{\circ}C$), $M^{-1}\,s^{-1}$	$\Delta H^{\ddagger}_{2}$, kcal/mol	$\Delta S^{\ddagger}_{2}$, cal/(K mol)	$10^{3}k_{-1}$ ($25\,^{\circ}C$), $M^{-1}\,s^{-1}$	$\Delta H^{\ddagger}_{-1}$, kcal/mol	$\Delta S^{\ddagger}_{-1}$, cal/(K mol)	$10^{3}k_{-2}$ ($25\,^{\circ}C$), s^{-1}	$\Delta H^{\ddagger}_{-2}$, kcal/mol	$\Delta S^{\ddagger}_{-2}$, cal/(K mol)
1	4-$CH_3OC_6H_4$	CH_3	2.0	13.7	−12	1.1	7.0 (1.0)	−21 (3)	1.3	10.8 (2.1)	−36 (7)	4.6	16.0 (0.4)	−16 (2)
2	4-$CH_3C_6H_4$	CH_3	4.3	11.7	−17	1.3	5.5 (1.4)	−27 (5)	3.0	11.2 (1.4)	−33 (5)	3.5	16.8 (0.8)	−14 (3)
3	C_6H_5	CH_3[b]	1.4	16.5	−2	0.67	6.6 (0.1)	−23 (1)	2.8	15.5 (0.5)	−19 (2)	2.7	13.6 (0.5)	−24 (3)
4	4-$NO_2C_6H_4$	CH_3	1.1	13.5	−14	1.1	7.4 (0.9)	−20 (3)	3.6	12.6 (3.9)	−28 (8)	8.1	15.2 (1.2)	−17 (4)
5	CH_3	4-$C_6H_4CH_3$	2.2	11.8	−18	1.0	2.7 (1.5)	−36 (6)	7.5	8.3 (0.7)	−40 (2)	10.2	15.5 (0.7)	−16 (3)
6	CH_3	C_6H_5[c]	1.5	15.3	−5	0.70	11.4 (0.6)	−7 (2)	6.7	16.3 (2)	−14 (1)	11.1	15.6 (0.1)	−15 (1)
7	CH_3	4-C_6H_4I	2.0	15.0	−7	1.0	6.1 (1.1)	−24 (4)	11.0	10.2 (1.1)	−33 (9)	12.8	14.8 (0.6)	−18 (1)
8	CH_3	4-C_6H_4Cl	1.3	14.3	−8	0.85	7.2 (2.7)	−20 (2)	10.4	10.5 (0.4)	−32 (1)	12.2	18.1 (1.7)	−7 (5)
9	CH_3	3-C_6H_4I	1.6	14.8	−9	0.62	6.3 (2.0)	−24 (4)	9.9	9.9 (1.3)	−34 (3)	11.4	17.3 (1.5)	−9 (3)
10	CH_3	3-C_6H_4CN	1.3	15.9	−6	0.48	9.4 (1.3)	−15 (4)	14.5	12.3 (2.0)	−26 (1)	20.3	16.0 (3.0)	−13 (4)
11	CH_3	4-$C_6H_4C(O)CH_3$	1.2	16.0	−6	0.46	12.4 (1.0)	−5 (2)	12.0	12.1 (2.5)	−27 (2)	16.7	15.0 (1.0)	−16 (2)
12	CH_3	4-C_6H_4CN	0.77	17.9	−0.5	0.50	4.2 (1.0)	−32 (3)	14.3	11.0 (1.2)	−31 (4)	18.2	15.4 (1.0)	−15 (4)
13	4-$CH_3OC_6H_4$	H[d]	4.7	14.0	−9	2.5	3.0 (0.8)	−33 (3)	19.0	11.1 (0.9)	−29 (3)	29.1	19.7 (0.3)	0 (1)

[a] Rate constants k_2, k_{-2}, and k_{-1} calculated from k_{exptl}^{rel} values (Tables II–XII[31]) obtained at 25 °C from eq 12. Associated activation parameters obtained from k_2, k_{-2}, and k_{-1} calculated from k_{exptl}^{rel} over a temperature range (Tables II–XII[31]). Rate constants k_1 calculated from the expression $k_1 = Q_f k_{-1}$; Q_f values listed in Table I; $\Delta H^{\ddagger}_{1}$ and $\Delta S^{\ddagger}_{1}$ values calculated from ΔH_f°, ΔS_f° (Table I) and $\Delta H^{\ddagger}_{-1}$, $\Delta S^{\ddagger}_{-1}$ values; all data at $I = 2.00$ M ($NaClO_4/HClO_4$). [b] Reference 6. [c] Redetermination of 25 °C data from that reported in ref 6. [d] Reference 39.

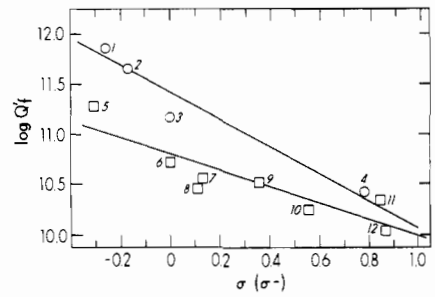

Figure 2. □: Plot of log Q_f' for reaction 9 vs. Hammett σ^- parameter for the substituent Y for substituted *N*-phenylacetohydroxamic acids, $CH_3C(O)N(OH)C_6H_4Y$ (R_2 series) (slope (ρ) = 1). ○: Plot of log Q_f' for reaction 9 vs. Hammett σ parameter for the substituent Y for substituted *N*-methylbenzohydroxamic acids, $YC_6H_4C(O)N(OH)CH_3$ (R_1 series) (slope (ρ) = 1.4). Numerical labels for data points are as defined in Table I.

substituent, Y, has been varied from electron donor to electron acceptor in the meta position, where inductive effects are possible, and the para position, where resonance and inductive effects are possible. Through the systematic variation of the substituent we have attempted to determine which features influence the relative stability of these complexes.

Mono(hydroxamato)iron(III) complex thermodynamic stability follows a definite trend as the substituents, Y, are varied from electron donor to electron acceptor. This trend is illustrated in Figure 2, which is a plot of the equilibrium quotient for eq 9 (Q_f') plotted as a function of the Hammett parameter (σ^-) where the slope, ρ is 1.0. The Hammett σ^- parameter measures the ability of a substituent to delocalize a lone pair of electrons adjacent to a phenyl ring.[33] Figure 2 illustrates that the stability of the iron(III) complex (Q_f') increases with the electron donor ability of Y. A similar trend is observed for Q_f.

This trend can be interpreted in terms of the substituent's ability to delocalize the lone pair of electrons on the nitrogen atom. Three resonance forms (III–V) illustrate this. We have

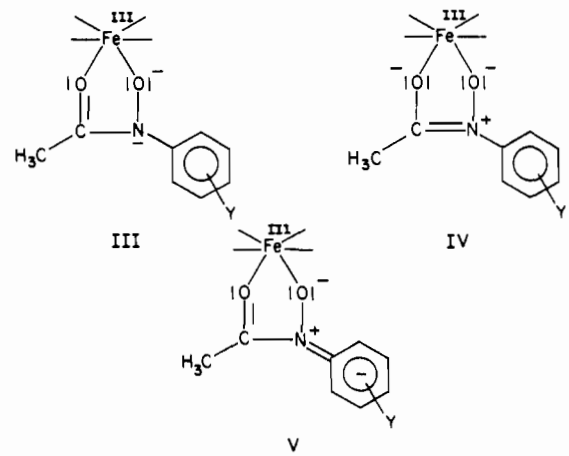

previously noted the influence of the delocalization of the N atom lone pair of electrons on complex stability.[6] X-ray structural analyses support a contribution from IV to the iron chelate structure. Crystal structures of $Fe(CH_3C(O)N(O)$-4-$CNC_6H_4)_3$ and the uncomplexed hydroxamic acid have been reported.[34] These structures show a decrease in C–N and increase in C–O bond distances on going from the free to the complexed hydroxamic acid. Similar bond length changes are observed on coordination of the trihydroxamate siderophore

(33) Leffler, J. E.; Grunwald, E. "Rates and Equilibria of Organic Reactions"; Wiley: New York, 1963.
(34) Mocherla, R. R.; Powell, D. R.; Barnes, C. L.; van der Helm, D. *Acta Crystallogr., Sect. C: Cryst. Struct. Commun.* **1983**, *C39*, 868.

deferriferrioxamine E to iron(III).[35,36] X-ray structural data are also consistent with R_1 and R_2 influencing this lone electron pair delocalization. Deferriferrioxamine E[36] and *N,N'*-dihydroxy-*N,N'*-diisopropylhexanediamide,[37] which have electron-releasing alkyl R_2 substituents, have shorter C–N and longer C–O bond distances than does $CH_3C(O)N(OH)$-4-CNC_6H_4,[34] which has an electron-withdrawing R_2 substituent. A similar trend is observed for $Fe(C_6H_5C(O)N(O)H)_3$[38] and $Fe(CH_3C(O)N(O)$-4-$CNC_6H_4)_3$,[34] but to a smaller degree.

For the R_2 series reported here, as Y becomes more electron donating, resonance form IV becomes more important relative to resonance forms III and V. The lone pair of electrons on nitrogen is delocalized toward the C–N bond, resulting in an increase in electron density on the carbonyl oxygen (relative to resonance forms III and V). This in turn is expected to enhance the carbonyl oxygen–iron bond strength, which results in the higher stability constants. Conversely, as Y becomes more electron accepting, resonance form V increases in importance and electron density is delocalized away from the carbonyl oxygen relative to resonance forms III and IV. This results in a decreased carbonyl oxygen–iron bond strength and hence lower complex stability.

Further support for the R_2 substituent affecting the carbonyl oxygen more than the N–O oxygen comes from an investigation of the influence of the R_2 substituent on the uncomplexed hydroxamic acid pK_a. A plot of pK_a vs. σ^- gives a slope ($\rho \sim 0.1$)[21] significantly less than that in Figure 2 ($\rho \sim 1.0$). If the hydroxyl oxygen were being influenced strongly by the substituent, Y, then one would expect that influence to be approximately the same for both reactions 8 and 9. The smaller ρ value for reaction 8 indicates that the hydroxyl oxygen is not being influenced as strongly as the carbonyl oxygen. This interpretation is consistent with resonance forms III–V.

Figure 3 is a plot of enthalpy change (ΔH) vs. entropy change (ΔS) for the acid dissociation reaction 8 (K_a) and the complex dissociation reaction 9 ($1/Q_f'$). Included in this plot are the enthalpy and entropy data for the R_2 and R_1 series and data determined in this laboratory[6,39] for another series of hydroxamic acids where R_1 = CH_3, C_6H_5, and 4-$CH_3OC_6H_4$ and R_2 = CH_3, C_6H_5, and H. As discussed elsewhere,[21,22,40] the position of the ligands on the plot for the acid dissociation reaction 8 (K_a) can be understood in terms of solvent–anion interaction. The relative positions of the complexes on the $1/Q_f'$ plot (Figure 3B) generally correspond to the positions of the ligands on the K_a plot (Figure 3A). This may suggest that complex stability should be discussed not only in terms of Fe^{3+}–hydroxamate bond strength but also in terms of solvation of the free hydroxamate anion.

Equilibrium Studies: R_1 Series. The electronic influence of the R_1 functional group on the thermodynamics of iron(III) complex formation was investigated on the series of hydroxamic acids I, where R_2 = CH_3 and R_1 = 4-C_6H_4Y (Y = NO_2, CH_3, H, CH_3O). Mono(hydroxamato)iron(III) complex thermodynamic stability follows the same trend as was found for the R_2 series. That is, as Y becomes a stronger electron donor, complex stability increases. Figure 2 includes a plot of log Q_f' vs. the Hammett σ parameter[33] for the R_1 series with a slope (ρ) of 1.4. σ parameters were used for this plot since the R_1 series more closely resembles the standard Hammett reaction series. The Q_f values for reaction 7 illustrate the same trend, but with a smaller ρ value (ρ = 0.7). Three new resonance forms (VI–VIII) may be used to interpret these results for the R_1 series. When Y is $-OCH_3$, resonance form VII is of increased importance. The negative formal charge density on the carbonyl oxygen is most likely responsible for the larger observed stability constants. Resonance form VIII is of increased relative importance when Y = NO_2. This resonance electron delocalization away from the carbonyl oxygen atom causes the relatively smaller stability constants.

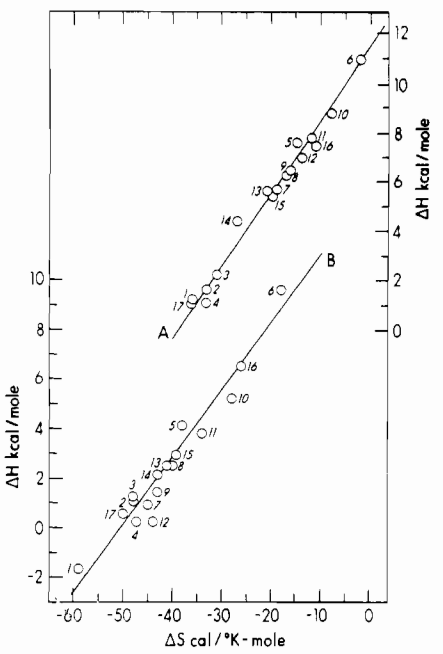

Figure 3. Plot of ΔH vs. ΔS: (A) reaction 8 (K_a); (B) reverse of reaction 9 ($1/Q_f'$). Data points numbered 1–13 are for hydroxamic acid ligands as defined in Tables I and XIII. Data points 14–17 are from ref 6: $CH_3C(O)N(OH)H$ (**14**); $C_6H_5C(O)N(OH)H$ (**15**); $C_6H_5C(O)N(OH)C_6H_5$ (**16**); $CH_3C(O)N(OH)CH_3$ (**17**).

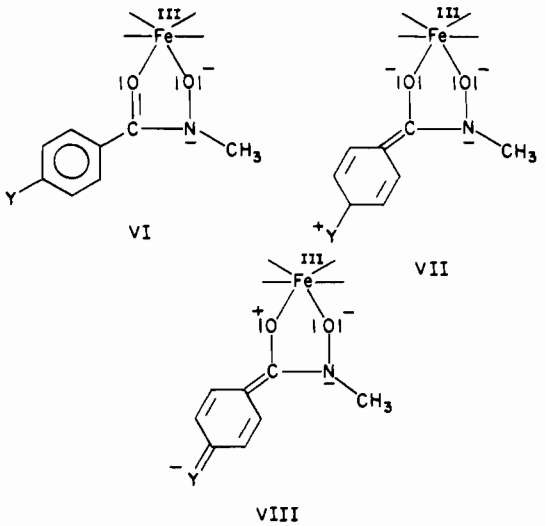

Kinetics and Mechanism. Intimate Mechanism. The validity of the parallel-path mechanism shown in Scheme I has been established. As noted above, due to the weak acidity of the hydroxamic acid ligands and the high $[H^+]$ of our experiments, path 3 may be unambiguously eliminated from our consideration. Thermodynamic and kinetic data are internally consistent as ΔG values (Tables I and XIII) computed indirectly for a particular path compare favorably with those directly observed.

The formation rate constants k_1 and k_2 (Table XIII) fall in a narrow range that is normally observed for monodentate

(35) van der Helm, D.; Poling, M. *J. Am. Chem. Soc.* **1976**, *98*, 82.
(36) Hossain, M. B.; van der Helm, D.; Poling, M. *Acta Crystallogr., Sect. B: Struct. Crystallogr. Cryst. Chem.* **1983**, *B39*, 258.
(37) Smith, W. L.; Raymond, K. N. *J. Am. Chem. Soc.* **1980**, *102*, 1252.
(38) Lindner, H. J.; Göttlicher, S. *Acta Crystallogr., Sect. B: Struct. Crystallogr. Cryst. Chem.* **1969**, *B25*, 832.
(39) Fish, L. L.; Crumbliss, A. L. *Inorg. Chem.*, in press.
(40) Monzyk, B.; Crumbliss, A. L. *J. Org. Chem.* **1980**, *45*, 4670.

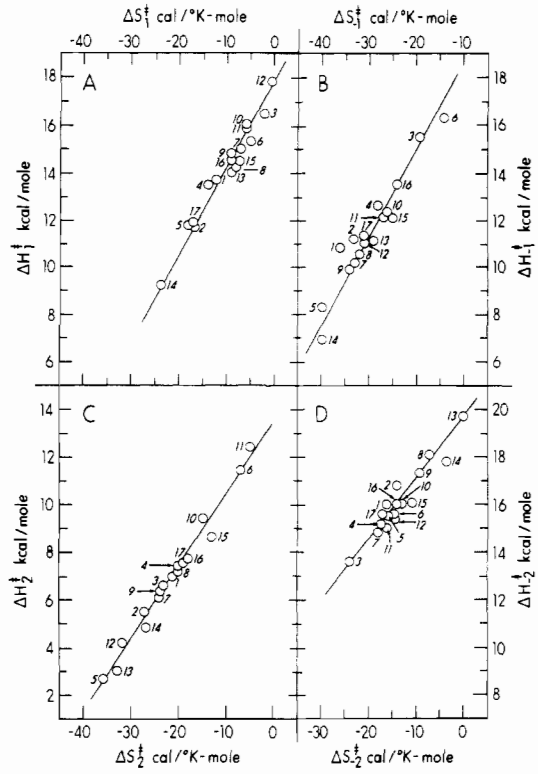

Figure 4. Isokinetic plots for the forward and reverse directions of path 1 [(A) $\Delta H^{\ddagger}_1$ vs. $\Delta S^{\ddagger}_1$ and (B) $\Delta H^{\ddagger}_{-1}$ vs. $\Delta S^{\ddagger}_{-1}$] and path 2 [(C) $\Delta H^{\ddagger}_2$ vs. $\Delta S^{\ddagger}_2$ and (D) $\Delta H^{\ddagger}_{-2}$ vs. $\Delta S^{\ddagger}_{-2}$]. Numerical labels for data points are as defined in the legend for Figure 3.

ligand substitution on $Fe(H_2O)_6^{3+}$ and $Fe(H_2O)_5OH^{2+}$, suggesting that initial bond formation is rate determining and that ring closure is rapid.[41] Figure 4 is a compilation of activation parameters for the forward and reverse direction of path 1 and path 2 for the 12 hydroxamic acids reported here (see also Table XIII). Also included in the plot are other hydroxamic acid ligands studied in this laboratory.[6,39] Both reaction paths in the forward and reverse direction exhibit a linear relationship between $\Delta H^{\ddagger}$ and $\Delta S^{\ddagger}$ over a wide range of values, which suggests that all the hydroxamic acids react via the same mechanism.[42] Furthermore, the activation parameters appear to be compensating,[43] which may be responsible for the small range of rate constants observed.

The interchange mechanism suggests that the second-order rate constant for complex formation (k_1, k_2) (eq 13 and 14)

$$k_1 = K_{os1}k_1^{*} = K_{os1}Sk_{ex}(Fe(H_2O)_6^{3+}) \quad (13)$$

$$k_2 = K_{os2}k_2^{*} = K_{os2}Sk_{ex}(Fe(H_2O)_5OH^{2+}) \quad (14)$$

should be related to an outer-sphere encounter complex association constant, K_{os}, and a first-order rate constant, k^{*}, associated with the collapse of the encounter complex to form the ligand-substituted product.[42,48,49] The constant k^{*} is related to the water-exchange rate constant, $k_{ex}(Fe(H_2O)_6^{3+})$ or $k_{ex}(Fe(H_2O)_5OH^{2+})$, by a statistical factor, S, due to solvation shell composition.

It is therefore useful to compare rate data for ligand substitution with that for water exchange when considering the intimate mechanism. Kinetic data for water exchange on $Fe(H_2O)_6^{3+}$ and $Fe(H_2O)_5OH^{2+}$ have been reported.[50,51] Pressure effects have been studied to obtain $\Delta V^{\ddagger}$ values, and on this basis water exchange on $Fe(H_2O)_6^{3+}$ and $Fe(H_2O)_5OH^{2+}$ is thought to proceed via I_a and I_d mechanism, respectively.[52] K_{os} is not known for our systems, but since the entering ligand is uncharged it may reasonably be assumed that K_{os} for $Fe(H_2O)_2^{3+}$ (path 1) and $Fe(H_2O)_5OH^{2+}$ (path 2) is the same. Hence, for the interchange mechanism to apply, then $k_2/k_1 \sim k_{ex}(Fe(H_2O)_5OH^{2+})/k_{ex}(Fe(H_2O)_6^{3+})$. The k_2/k_1 range for the 17 hydroxamic acid systems investigated in our laboratory is 300–2300, with an average value of 720 (σ = 525). This is in reasonable agreement with the reported value for $k_{ex}(Fe(H_2O)_5OH^{2+})/k_{ex}(Fe(H_2O)_6^{3+})$ of 750[50] and demonstrates the applicability of the interchange mechanism to our system but leaves open the possibility for some entering group participation in the transition states.

If one assumes that $K_{os1} = 0.1$[53] for path 1, then k_1^{*} (eq 13) is calculated to vary by a factor of 7 from 11 to 77 s^{-1}. As noted above this small range in k_1^{*} is due to compensating $\Delta H^{\ddagger}_1$ and $\Delta S^{\ddagger}_1$ effects (Figure 4). The range of activation parameter values suggests there is some entering-group effect. Comparison with the energetics of water exchange for $Fe(H_2O)_6^{3+}$ is again useful. It has been argued that the less dissociative a reaction mechanism, the lower is $\Delta H^{\ddagger}$.[54] Reported $\Delta H_{ex}^{\ddagger}$ values for water exchange at $Fe(H_2O)_6^{3+}$ are 15.3[51] and 18.5[50] kcal/mol. The inequality $\Delta H^{\ddagger}_1 \leq \Delta H_{ex}^{\ddagger}$ holds for all 17 hydroxamic acids, using 18.5 kcal/mol for water exchange, and within experimental error for 16 hydroxamic acids, using the lower value for water exchange. This suggests some entering-group bond formation in the transition state for path 1. The negative $\Delta S^{\ddagger}_1$ values are also consistent with entering-group participation in the transition state, although C–N bond rotation necessary to convert the hydroxamate ligand from a trans to a cis configuration for chelate formation may also contribute to the entropy decrease. Calculation values for k_1^{*} are significantly less than k_{ex} for $Fe(H_2O)_6^{3+}$,[50,51] suggesting that H_2O dissociation from $Fe(H_2O)_6^{3+}$ is still energetically dominant. The average statistical correction, S, in eq 13 is 0.15. This relatively low value[55] may be a result of the steric bulk and trans–cis C–N bond rotation requirements of the hydroxamic acid entering ligand.

Kinetic data for the reverse reaction in path 1 support some hydroxamic acid ligand participation in the transition state. The negative $\Delta S^{\ddagger}_{-1}$ values are consistent with incomplete dissociation of the hydroxamate ligand in the transition state. Consideration of a linear free energy relationship (LFER)

(41) Margerum, D. W.; Cayley, G. R.; Weatherburn, D. C.; Pagenkopf, G. K. In "Coordination Chemistry"; Martell, A. E., Ed.; American Chemical Society: Washington, DC, 1978; ACS Monogr. No. 174, Vol. 2, p 1.
(42) Wilkins, R. G., "The Study of Kinetics and Mechanism of Reactions of Transition Metal Complexes"; Allyn and Bacon: Boston, 1974.
(43) The linear correlations between $\Delta H^{\ddagger}$ and $\Delta S^{\ddagger}$ shown in Figure 4 do not conform to the strict statistical criteria established by Krug[44] and Exner[45] for a true isokinetic relationship. However, we have applied the error analysis described by Petersen et al.[46] and Wiberg[47] to these data that shows that the $\Delta H^{\ddagger}$ and $\Delta S^{\ddagger}$ ranges observed are statistically significant and the linear correlations valid. Consequently the range and number of data points for each correlation are suffficiently large for us to suggest that a compensating effect is operating for both paths 1 and 2.
(44) Krug, R. R. *Ind. Eng. Chem. Fundam.* **1980**, *19*, 50.
(45) Exner, O. *Collect. Czech. Chem. Commun.* **1972**, *37*, 1425; **1975**, *40*, 2762; *Prog. Phys. Org. Chem.* **1973**, *10*, 411.
(46) Petersen, R. C.; Markgraf, J. H.; Ross, S. D. *J. Am. Chem. Soc.* **1961**, *83*, 3819.
(47) Wiberg, K. B. "Physical Organic Chemistry"; Wiley: New York, 1964; pp 376–379.
(48) Langford, C. H.; Gray, H. B. "Ligand Substitution Dynamics"; W. A. Bejamin: New York, 1965.
(49) Eigen, M. In "Advances in the Chemistry of Coordination Compounds"; Kischner S., Ed.; Macmillan: New York, 1961; p 371.
(50) Dodgen, H. W.; Liu, G.; Hunt, J. P. *Inorg. Chem.* **1981**, *20*, 1002.
(51) Grant, M.; Jordan, R. B. *Inorg. Chem.* **1981**, *20*, 55.
(52) Swaddle, T. W.; Merbach, A. E. *Inorg. Chem.* **1981**, *20*, 4212.
(53) Fuoss, R. M. *J. Am. Chem. Soc.* **1958**, *80*, 5059. Prue, J. E. *J. Chem. Educ.* **1969**, *46*, 12.
(54) Tanaka, M. *Inorg. Chim. Acta* **1981**, *54*, L129.
(55) Neely and Connick[56] propose 0.75 as a reasonable value for S, although other authors have suggested lower values.[57]
(56) Neely, J.; Connick, R. *J. Am. Chem. Soc.* **1970**, *92*, 3476.
(57) Langford, C. H. *J. Chem. Educ.* **1969**, *46*, 557.

between $\Delta G^{\ddagger}$ and ΔG° is sometimes used as a method of elucidating the intimate mechanism of a dissociation reaction. A direct correlation of the form $\Delta(\Delta G^{\ddagger}) = \alpha\Delta(\Delta G^{\circ}) + c$, where $\alpha = 1.0$ and c is a constant for a series of dissociation reactions, has been interpreted in terms of an I_d mechanism.[58,59] The corresponding plots of $\Delta G^{\ddagger}_{-1}$ vs. ΔG° for the hydroxamic acids reported here and elsewhere[6,39] show considerable scatter. This is not consistent with an I_d mechanism but is consistent with transition-state free energies that are dependent upon variations in leaving group, as would be the case for an I_a process.[60]

Our results for path 1, based on an analysis of rate and equilibrium constants and activation parameters for the forward and reverse reactions, support hydroxamic acid ligand participation in the transition state and are thus consistent with an I_a mechanism. Previous authors have also proposed an I_a mechanism for ligand substitution at $Fe(H_2O)_6^{3+}$ on the basis of a ligand dependence for k_f[42,51,61-65] or an interpretation of activation volumes.[13,52,66,67]

Parameters relating to ligand influence in path 2 show trends similar to those found for path 1. Assuming a value for K_{os2} of 0.1 M^{-1}, calculated $k_2^{\ddagger}$ values (eq 14) vary by a factor of 9 from 4.6 to 43 s^{-1}. This is a minimal variation to imply any significant hydroxamic acid entering ligand participation in the transition state; however, as noted above, compensating $\Delta H^{\ddagger}_2$ and $\Delta S^{\ddagger}_2$ values (Figure 4) would tend to dampen ligand influence on $k_2^{\ddagger}$. The following observations are all consistent with some hydroxamic acid ligand participation in the transition state for path 2: (1) $\Delta H^{\ddagger}_2 \leq \Delta H_{ex}^{\ddagger}$ for $Fe(H_2O)_5OH^{2+}$[51] for 15 of 17 hydroxamic acids. (2) $\Delta H^{\ddagger}_2$ varies significantly with hydroxamic acid ligand. (3) $\Delta S^{\ddagger}_2$, $\Delta S^{\ddagger}_{-2} < 0$. (4) A plot of $\Delta G^{\ddagger}_{-2}$ vs. ΔG° shows considerable scatter. Consequently, we conclude that ligand substitution via path 2 has I_a characteristics.

However, current interpretation of pressure effects on H_2O substitution rates ($\Delta V^{\ddagger}$) for $Fe(H_2O)_5OH^{2+}$[52] is that this process proceeds by an I_d mechanism. Several other authors have interpreted ligand substitution on $Fe(H_2O)_5OH^{2+}$ to proceed by an I_d mechanism on the basis of a lack of variation in the observed second-order formation rate constant[41,42,61,63,68,69] and positive $\Delta V^{\ddagger}$ values.[13,66,67] The fact that our calculated $k_2^{\ddagger}$ values are considerably less than k_{ex} for $Fe(H_2O)_5OH^{2+}$ suggests that H_2O dissociation is energetically dominant in the ligand-substitution process; the average statistical factor S computed for path 2 is 0.1 (eq 14). The negative $\Delta S^{\ddagger}_2$ values may arise partly from steric requirements of trans–cis C–N bond rotation within the encounter complex and/or from a H-bonded preequilibrium step involving coordinated –OH as shown in Scheme II.

Tanaka and co-workers[13] have obtained $\Delta V^{\ddagger}_2$ data for the reaction of acetohydroxamic acid with $Fe(H_2O)_5OH^{2+}$ and on the basis that $\Delta V^{\ddagger}_2 > 0$ have assigned an I_d mechanism to that process. The range of $\Delta H^{\ddagger}$ and $\Delta S^{\ddagger}$ values, compensation effects, and lack of $\Delta G^{\ddagger}_{-2} - \Delta G^{\circ}$ correlations reported here for a homologous series of ligands, however, suggests the possibility for some associative character in path 2. Furthermore, interpretations of $\Delta V^{\ddagger}$ data are not unequivocal.[70] The calculated values for $\Delta V^{\ddagger}$ are a sum of contributions from outer-sphere complex formation (ΔV_{os}°), solvation effects ($\Delta V_{solv}^{\ddagger}$), and that associated with the actual substitution process, i.e. the collapse of the encounter complex ($\Delta V_{intr}^{\ddagger}$). It is the latter term that is of interest in mechanistic interpretations of the ligand-substitution process. Tanaka and co-workers[13] assume ΔV_{os}° and $\Delta V_{sol}^{\ddagger}$ to be zero and therefore $\Delta V_{intr}^{\ddagger} > 0$. However, a preequilibrium H-bonding interaction as shown in Scheme II may free solvent molecules H bonded to coordinated –OH and make $\Delta V_{solv}^{\ddagger} > 0$. This would make $\Delta V_{intr}^{\ddagger}$ less positive and the interpretation of $\Delta V^{\ddagger}_2$ less certain. Results reported here and elsewhere in the literature emphasize that the distinction between an I_d and I_a mechanism is often a subtle one indeed.

Scheme II

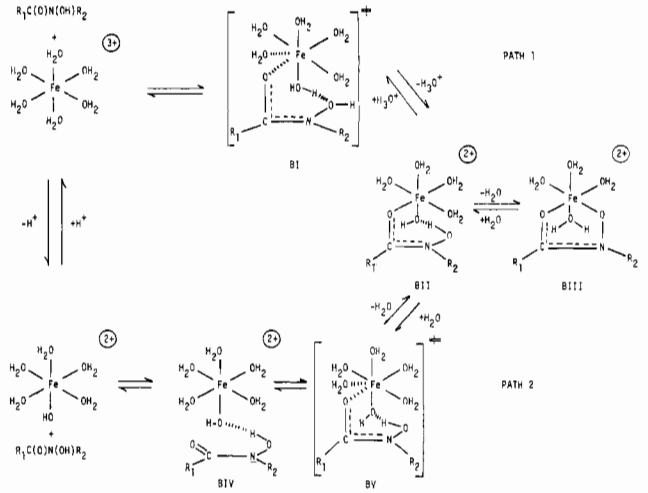

Reaction Scheme II represents the intermediates and transition states that may occur along the reaction coordinate for both path 1 and path 2. Focusing on path 2, structure BII represents the half-bonded form that, during complex formation, undergoes rapid ring closure to form BIII. On going from the complex (BIII) to the half-bonded structure (BII), protonation is implied for the hydroxamate ligand. This is due to the relative acidities of the hydroxamic acids ($pK_a \sim 9$) as compared with coordinated H_2O on Fe_{aq}^{3+} ($pK_a \sim 3$). The cyclic structure shown in BII and the transition-state structure corresponding to the rate-determining process (BV) are consistent with the negative values for $\Delta S^{\ddagger}_{-2}$ and $\Delta S^{\ddagger}_2$. This associative character for complex formation could arise as a result of one or both of the following: partial Fe–carbonyl oxygen bond formation in the transition state (BV) (i.e., an I_a process) and/or a H-bonding interaction that might occur in a preequilibrium step (BIV). As suggested previously,[6] initial bond formation is shown to occur at the carbonyl O atom in both path 1 and path 2. This is consistent with the kinetic influence of the R_1 and R_2 substituents as presented below.

In aquation via path 1, the half-bonded intermediate (BII) undergoes protonation. This step is expected to be fast relative to Fe–carbonyl oxygen bond breakage and most likely occurs at the hydroxyl oxygen on Fe^{3+}. This O–H bond formation contribution should lower the enthalpy of activation relative to the acid-independent path. This is consistent with results reported here and previously, in that for all except two of the 17 hydroxamic acids $\Delta H^{\ddagger}_{-1} \leq \Delta H^{\ddagger}_{-2}$. The more negative values for $\Delta S^{\ddagger}_{-1}$ (relative to $\Delta S^{\ddagger}_{-2}$) may arise as a result of

(58) Langford, C. H. *Inorg. Chem.* **1965**, *4*, 265.
(59) Haim, A. *Inorg. Chem.* **1970**, *9*, 426.
(60) It has been suggested[61] that α should change monotonically over an extensive series of related reactions that proceed via an I_a process.
(61) Swaddle, T. W. *Coord. Chem. Rev.* **1974**, *14*, 217.
(62) Mentasti, E.; Secco, F.; Venturini, M. *Inorg. Chem.* **1982**, *21*, 2314.
(63) Dash, A. C.; Harris, G. M. *Inorg. Chem.* **1982**, *21*, 2336.
(64) Mentasti, E.; Secco, F.; Venturini, M. *Inorg. Chem.* **1982**, *21*, 602.
(65) Perlmutter-Hayman, B.; Tapuhi, E. *J. Coord. Chem.* **1976**, *6*, 31.
(66) Jost, A. *Ber. Bunsenges. Phys. Chem.* **1976**, *80*, 316.
(67) Hasinoff, B. B. *Can. J. Chem.* **1976**, *54*, 1820; **1979**, *57*, 77.
(68) Mentasti, E. *Inorg. Chem.* **1979**, *18*, 1512.
(69) Magini, M.; Saltelli, A.; Caminiti, R. *Inorg. Chem.* **1981**, *20*, 3564.
(70) See for example: Swaddle, T. W. *Inorg. Chem.* **1980**, *19*, 3203. Newman, K. E.; Merbach, A. E. *Inorg. Chem.* **1980**, *19*, 2481. Lawrence, G. A.; Stranks, D. R. *Acc. Chem. Res.* **1979**, *12*, 403.

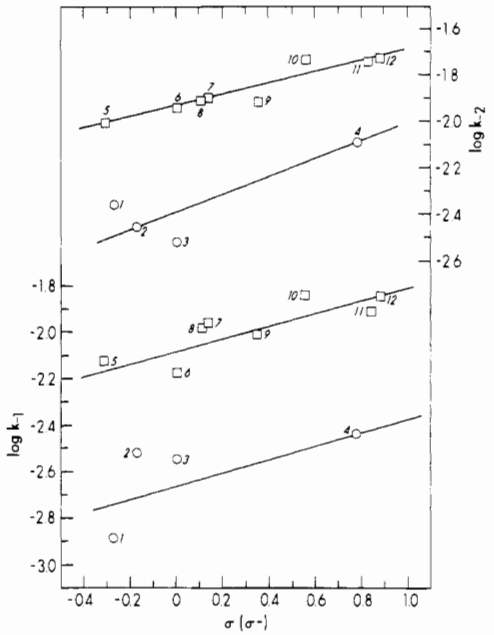

Figure 5. □: Plot of log k_{-2} and log k_{-1} for the reverse of reactions 5 and 7 vs. Hammett σ^- parameter for the substituent Y for the substituted *N*-phenylacetohydroxamic acids, $CH_3C(O)N(OH)C_6H_4Y$ (R_2 series). O: Plot of log k_{-2} and log k_{-1} for the reverse of reactions 5 and 7 vs. Hammett σ parameter for the substituent Y for the substituted *N*-methylbenzohydroxamic acids, $YC_6H_4C(O)N(OH)CH_3$ (R_1 series). Numerical labels for hydroxamic acid data points are as defined in Table XIII.

bringing together a 1+ and a 2+ species in forming the transition state (BI). In line with the results of the acid-independent aquation reaction (path 2), one would expect the enthalpy of activation ($\Delta H^{\ddagger}_{-1}$) for the Fe–carbonyl oxygen bond cleavage to vary with changes in the substituents on R_1 and R_2. This is consistent with our results. If initial bond formation occurred at the hydroxyl oxygen, we would not expect to see this variation in $\Delta H^{\ddagger}_{-1}$, as our evidence is that the hydroxyl oxygen is not strongly influenced by the substituents on R_1 and R_2.[21,40]

Relative Influence of the R_1 and R_2 Groups. We now turn to a consideration of the relative influence of the R_1 and R_2 substituent on the kinetic and thermodynamic stability of the iron(III) complex. Our previous report,[6] which permuted C_6H_5, CH_3, and H in the R_1 and R_2 positions, pointed out the importance of the R_2 substituent and its ability to enhance the delocalization of the lone pair of electrons on N into the C–N bond. The hydroxamic acids reported here were selected to test the relative influence of electron-donating and -withdrawing substituted phenyl groups in the R_1 and R_2 position. As noted above, for the R_2 substituent only inductive electron donation is possible, while both inductive and resonance electron withdrawal are possible. For the R_1 substituent both inductive and resonance electron donation and withdrawal are possible.

Figure 5 is a plot of dissociation rate constants for paths 1 and 2 (k_{-1}, k_{-2}) as a function of σ and σ^- parameters for the R_1 and R_2 series. The linear correlation in both cases illustrates that as the R_1 or R_2 substituent becomes more electron donating, dissociation rates become slower. (The relatively greater scatter in the data for path 1 may be a result of the more complex pre-rate-determining protonation step.) The resonance forms (III–V for the R_2 series and VI–VIII for the R_1 series) used to describe the thermodynamic data may also be used to interpret the kinetic data. As Y becomes more electron donating, resonance form IV for the R_2 series and VII for the R_1 series become relatively more important. For both resonance forms, electron density is delocalized toward the carbonyl oxygen atom. We have previously argued that the rate-limiting dissociation process for mono(hydroxamato)-iron(III) complexes is cleavage of the carbonyl oxygen–iron bond as shown in Scheme II.[6] Consequently, this delocalization of electron density toward the carbonyl oxygen atom should lower the dissociation rate constant. Conversely, as the substituent becomes relatively more electron accepting, resonance form V for the R_2 series and resonance form VIII for the R_1 series become more important. This decrease in electron density at the carbonyl oxygen results in relatively larger dissociation rate constants.

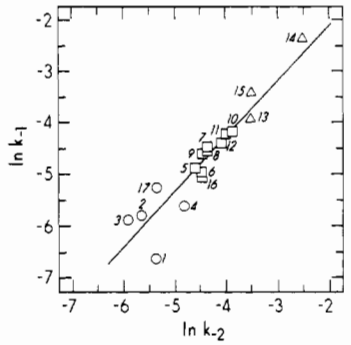

Figure 6. Plot of ln k_{-1} (reverse of reaction 7) vs. ln k_{-2} (reverse of reaction 5). Numerical labels for data points are as defined in the legend for Figure 3. Key: △, hydroxamic acids where R_2 = H; □, hydroxamic acids where $R_2 = C_6H_4Y$; O, hydroxamic acids where $R_2 = CH_3$.

The importance of the inductive electron-donating ability of the R_2 substituent is illustrated in Figure 6, which is a plot of ln k_{-1} vs. ln k_{-2}. This figure also includes iron(III)–hydroxamate dissociation rate data previously reported from our laboratory.[6] This linear plot with slope ca. 1 is consistent with similar aquation mechanisms and transition states that differ by a H^+ for the two parallel paths.[71] It is significant that for all 17 hydroxamic acid systems the dissociation rate constants group together in three regions according to whether R_2 = H (largest), substituted phenyl (intermediate), or CH_3 (smallest), *regardless of the R_1 substituent*. The ligands with $R_2 = CH_3$ having the lowest dissociation rate constants for path 1 or path 2 are consistent with the importance of inductive stabilization of N lone pair delocalization into the C–N bond.

The hydroxamic acid ligands chosen for the R_1 study (see I) were carefully picked so that possible resonance electron donation (Y = OCH_3) and resonance electron withdrawal (Y = NO_2) could be investigated. As well, Y = CH_3 was chosen so that the isomeric pair, 4-$CH_3C_6H_4C(O)N(OH)CH_3$ and $CH_3C(O)N(OH)$-4-$C_6H_4CH_3$, could be studied. The R_2 series was also designed so as to test the influence of electron-donating and -withdrawing substituted phenyl groups. The results of the R_1 series, the R_2 series, and the study completed in this laboratory where $R_1 = CH_3$ or C_6H_5 and R_2 = H, CH_3, or C_6H_5[6] have allowed us to determine in both kinetic and thermodynamic terms (1) what the "best" R_1 substituent is for complex stability, (2) what the "best" R_2 substituent is for complex stability, and (3) which group, R_1 or R_2, has the dominant influence on complex stability.

Figures 2 and 5 show that for the ligands that transpose $-C_6H_4Y$ and $-CH_3$ in the R_1 and R_2 positions the R_1 series gives iron(III) complexes that are thermodynamically and kinetically more stable and slightly more sensitive to the electronic influence of Y than the R_2 series. However, a complication is that the R_1 series reported here has a $-CH_3$ group on R_2 that is capable of enhancing N atom lone electron pair delocalization into the C–N bond and is thus responsible

(71) Asher, L. E.; Deutsch, E. Inorg. *Chem.* **1973**, *12*, 1774.

Table XIV. Influence of the R_2 Substituent

no.	$R_1C(O)N(OH)R_2$ R_1	R_2	log Q_f'	log k_{-1}	log k_{-2}	ref
14	CH_3	H	10.93	−1.04	−1.10	*a*
17	CH_3	CH_3	11.37	−2.28	−2.32	*a*
6	CH_3	C_6H_5	10.69	−2.18	−1.95	*b*
15	C_6H_5	H	10.68	−1.47	−1.45	*a*
3	C_6H_5	CH_3	11.02	−2.55	−2.57	*a*
16	C_6H_5	C_6H_5	10.41	−2.16	−1.90	*a*
13	4-$CH_3OC_6H_4$	H	11.16	−1.72	−1.54	*c*
1	4-$CH_3OC_6H_4$	CH_3	11.86	−2.89	−2.34	*b*
4	4-$NO_2C_6H_4$	CH_3	10.41	−2.44	−2.09	*b*

[a] Reference 6. [b] This work; see Tables I and XIII. [c] Reference 39.

Table XV. Comparison of Isomeric Ligand Pairs

no.	$R_1C(O)N(OH)R_2$ R_1	R_2	log Q_f'	log k_{-1}	log k_{-2}	ref
6	CH_3	C_6H_5	10.69	−2.18	−1.95	*a*
3	C_6H_5	CH_3	11.02	−2.55	−2.57	*b*
5	CH_3	4-$CH_3C_6H_4$	11.28	−2.12	−1.99	*a*
2	4-$CH_3C_6H_4$	CH_3	11.66	−2.52	−2.45	*a*

[a] This work; see Tables I and XIII. [b] Reference 6.

for the enhanced kinetic (see Figure 6) and thermodynamic stability. This point may be illustrated further by considering the Q_f', k_{-1}, and k_{-2} values for the iron(III)–hydroxamate complexes listed in Table XIV. When $R_1 = CH_3$, C_6H_5, or 4-$CH_3OC_6H_4$, substituting $R_2 = CH_3$ for $R_2 = H$ enhances the kinetic and thermodynamic stability of the iron(III) complex more than when $-C_6H_5$ is substituted for $-H$ in the R_2 position (compare entries **14**, **17**, **6**; **15**, **3**, **16**; **13**, **1** in Table XIV). In addition, for $C_6H_5C(O)N(OH)H$ substituting $R_2 = CH_3$ for $R_2 = H$ decreases k_{-1} and k_{-2} by 1 order of magnitude (compare entries **15** and **3** in Table XIV) compared to the case where placing the best electron donor on the R_1 phenyl group (4-$CH_3OC_6H_4C(O)N(OH)H$) produces only a very small decrease (compare entries **15** and **13** in Table XIV). Furthermore, consideration of thermodynamic and kinetic data (Table XV) for the two isomeric pairs of hydroxamic acid ligands

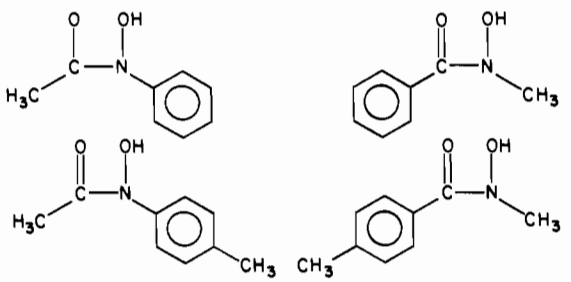

illustrates that when the $-CH_3$ group is placed in the R_2 rather than the R_1 position the thermodynamic and kinetic stability of the iron(III) complex is enhanced.

Therefore, we conclude that even though the R_1 series yields iron(III) complexes that are more stable (kinetically and thermodynamically) than the R_2 series, this is most likely largely due to the strong influence of the $R_2 = CH_3$ group in the R_1 series. The slightly greater sensitivity to changes in the R_1 substituent may be due to the fact that both inductive and resonance electron donation is effective at the R_1 position, although we cannot completely discount a possible effect of the $-CH_3$ group in the R_2 position.

Although the $R_2 = CH_3$ group is significant in thermodynamic and kinetic stabilization of the iron(III) complex, its effect with the R_1 substituent is additive. That is, even for the hydroxamic acid with the "best" R_1 group (4-$CH_3OC_6H_4C(O)N(OH)H$) the thermodynamic and kinetic stability may be further enhanced by placing a CH_3 group in the R_2 position (4-$CH_3OC_6H_4C(O)N(OH)CH_3$) (see **13** and **1** in Table XIV). Furthermore, it apparently is not possible to enhance the $R_2 = CH_3$ group's ability to inductively stabilize the N atom lone electron pair delocalization onto the C–N bond by putting an electron-withdrawing group in the R_1 position. This is evidenced by comparing the stability and dissociation rate constants for 4-$NO_2C_6H_4C(O)N(OH)CH_3$ with 4-$CH_3OC_6H_4C(O)N(OH)CH_3$ (entries **4** and **1** in Table XIV). In other words, the permutation that provides the best thermodynamic and kinetic stability is the case where both R_1 and R_2 are pushing electron density toward the carbonyl oxygen, as in 4-$CH_3OC_6H_4C(O)N(OH)CH_3$.

Table XVI. Influence of the R_1 Substituent

no.	$R_1C(O)N(OH)R_2$ R_1	R_2	log Q_f'	log k_{-1}	log k_{-2}	ref
1	4-$CH_3OC_6H_4$	CH_3	11.86	−2.89	−2.34	*a*
2	4-$CH_3C_6H_4$	CH_3	11.66	−2.52	−2.46	*a*
13	4-$CH_3OC_6H_4$	H	11.16	−1.72	−1.54	*c*
14	CH_3	H	10.93	−1.04	−1.10	*b*

[a] This work; see Tables I and XIII. [b] Reference 6. [c] Reference 39.

Now that it has been shown that the R_1 and R_2 effects are additive and that the R_2 effect must be inductive stabilization of the positive charge resulting from N atom lone electron pair delocalization into the C–N bond, we turn to the question as to whether the influence of the electron-donating substituted phenyl group in the R_1 position is primarily inductive or resonance. When $R_1 = CH_3OC_6H_4$ or $CH_3C_6H_4$ ($R_2 = CH_3$), the kinetic and thermodynamic data (entries **1** and **2**, Table XVI) are comparable, suggesting that both are acting in a similar manner, that is inductively. That $R_1 = CH_3OC_6H_4$ is not acting as a resonance donor may be the result of inhibition from $R_2 = CH_3$. The $R_1 = CH_3OC_6H_4$ group may contribute as a resonance donor when $R_2 = H$, however. That this is a possibility is suggested by comparing the thermodynamic and kinetic stability of $CH_3OC_6H_4C(O)N(OH)H$ and $CH_3C(O)N(OH)H$ (entries **13** and **14**, Table XVI), where in the latter case the $R_1 = CH_3$ group can only act inductively.

To summarize, the greatest complex stability, both thermodynamically and kinetically, is achieved when both the R_1 group and the R_2 group are capable of electron donation (e.g., $CH_3OC_6H_4C(O)N(OH)CH_3$). Both the R_1 and the R_2 groups influence complex stability, although the R_2 group plays the dominant role through inductive stabilization of N atom lone electron pair delocalization into the C–N bond. Limited data suggest that the R_1 group appears to be acting in an inductive manner when R_2 is an electron donor, although resonance donation may also contribute when the R_2 group is not an electron donor.

A final correlation can be made that illustrates our conclusion that both the R_1 and R_2 groups affect the electron density at the carbonyl oxygen atom. Figure 7 illustrates the influence of R_1 and R_2 on the affinity of the hydroxamate ion for $Fe(H_2O)_6^{3+}$ relative to H^+. Here the logarithm of the equilibrium quotient for reaction 9 (Q_f') has been plotted as a function of the logarithm of the equilibrium quotient for the reverse of reaction 8 (K_a^{-1}).[21,22,40] The extensive scattering of the data in the plot suggests that the R_1 and R_2 substituents influence iron(III) complex stability differently than they do pK_a values. If R_1 and R_2 were both affecting only the hydroxyl oxygen, then a reasonable correlation between log Q_f' and pK_a might be expected. However, variations in complex stability are influenced by electron density at both the carbonyl and hydroxyl oxygens, while pK_a variations should not be influenced by electron density at the carbonyl oxygen.

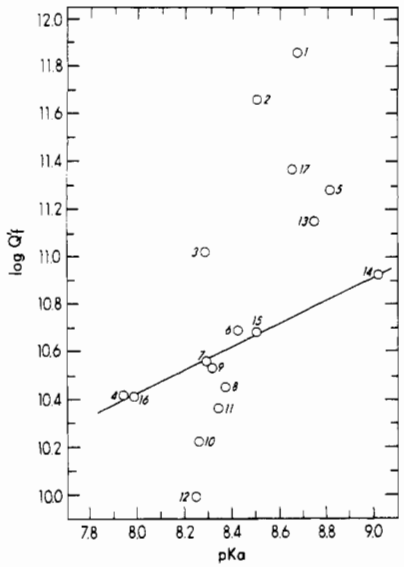

Figure 7. Plot of log Q_f' for reaction 9 vs. hydroxamic acid ligand pK_a (log K_a^{-1} for the reverse of reaction 8). Numerical labels for data points are as listed in the legend for Figure 3.

However, in spite of the scatter in Figure 7 some relevant trends are apparent. The relative magnitudes of Q_f' and K_a indicate that the hydroxamate ion has a greater affinity for Fe^{3+} than H^+, presumably due to the higher positive charge on Fe^{3+} and the chelate effect. The solid line in Figure 7 was arbitrarily drawn through data points for the simple hydroxamic acids $CH_3C(O)N(OH)H$ and $C_6H_5C(O)N(OH)H$ with a slope of 0.5. Inspection of this plot shows that those data points that fall above the line (i.e., those compounds that form more stable iron(III) complexes than might be expected on the basis of their pK_a values) correspond to hydroxamic acids either where both the R_1 and R_2 groups are electron donors or when either R_1 or R_2 is one of the "best" functional groups. In other words, when R_1 or R_2 is an electron donor, there is a buildup of negative charge density on the carbonyl oxygen atom, resulting in a greater affinity for Fe_{aq}^{3+}. This does not correspondingly enhance the hydroxamate ion's affinity for H^+ in aqueous solution, since protonation occurs at the hydroxyl oxygen. Conversely, all of the data points below the line in Figure 7 involve hydroxamic acids with R_2 groups that are capable of electron delocalization away from the carbonyl oxygen. These ligands have a lower affinity for Fe^{3+} than one would expect on the basis of their pK_a values because of the decreased electron density at the carbonyl oxygen.

Acknowledgment is made to the donors of the Petroleum Research Fund, administered by the American Chemical Society, for support of this research. We also thank L. L. Fish for making results available prior to publication.

Registry No. I (Y = H), 2446-50-6; I (Y = 4-NO_2), 1613-77-0; I (Y = 4-CH_3), 1613-85-0; I (Y = 4-CH_3O), 2614-48-4; II (Y = H), 1795-83-1; II (Y = 4-CH_3), 27451-21-4; II (Y = 4-Cl), 1503-91-9; II (Y = 4-I), 67274-49-1; II (Y = 3-I), 80584-64-1; II (Y = 4-CN), 80584-65-2; II (Y = 3-CN), 80584-66-3; II (Y = 4-$C(O)CH_3$), 67274-51-5; Fe, 7439-89-6; $Fe(H_2O)_6^{3+}$, 15377-81-8; $Fe(H_2O)_5(OH)^{2+}$, 15696-19-2.

Supplementary Material Available: Tables II-XII, giving rate constant data (30 pages). Ordering information is given on any current masthead page.

Contribution from the Department of Chemistry, Yale University, New Haven, Connecticut 06511

Selenido Osmium Carbonyl Cluster Compounds. Structure, Bonding, and Reactivity of the Electron-Rich Cluster $Os_4(CO)_{12}(\mu_3\text{-Se})_2$

RICHARD D. ADAMS*† and ISTVÁN T. HORVÁTH

Received March 19, 1984

The compound $HOs_3(CO)_{10}(\mu\text{-SePh})$ (**3**) has been prepared (75% yield) by the reaction of $Os_3(CO)_{10}(NCMe)_2$ with PhSeH. Under the conditions 160 °C (3000 psi CO), **3** eliminates benzene and is transformed into the compounds $Os_3(CO)_9(\mu_3\text{-Se})_2$ (**4**) and $Os(CO)_5$ in 95% yield. When irradiated (UV) under an atmosphere of CO, **3** loses benzene and is converted to $Os_3(CO)_9(\mu_3\text{-CO})(\mu_3\text{-Se})$ (**5**) in 18% yield. When irradiated in the presence of $Os(CO)_5$, **4** adds one $Os(CO)_4$ moiety to form the compound $Os_4(CO)_{13}(\mu_3\text{-Se})_2$ (**6**) in 33% yield. At 125 °C, **6** loses 1 mol of CO to form the cluster $Os_4(CO)_{12}(\mu_3\text{-Se})_2$ (**7**) quantitatively. **7** has been characterized by a single-crystal X-ray diffraction analysis: space group $P\bar{1}$ (No. 2), a = 13.987 (4) Å, b = 16.371 (6) Å, c = 9.491 (6) Å, α = 106.04 (4)°, β = 90.31 (4)°, γ = 81.63 (3)°, V = 2065 (3) Å^3, Z = 4, ρ_{calcd} = 4.036 g/cm^3. The structure was solved by direct methods and refined (4036 reflections, $F^2 \geq 3.0\sigma(F^2)$) to the final residuals R_F = 0.047 and R_{wF} = 0.056. The molecule consists of a butterfly tetrahedral cluster of four osmium atoms, with triply bridging selenido ligands bridging the two open triangular faces. The metal-metal bonding is irregular, with two of the five metal-metal bonds being greater than 3.00 Å in length. **7** adds 1 mol of CO under mild conditions (25 °C (1 atm CO)) to re-form **6** quantitatively. At 125 °C, **7** oxidatively adds 1 mol of H_2 to yield the compound $H_2Os_4(CO)_{12}(\mu_3\text{-Se})_2$ (**8**) in 35% yield. **5** reacts with H_2 at 125 °C to form $H_2Os_3(CO)_9(\mu_3\text{-Se})$ (**9**) in 39% yield.

Introduction

The thermally and photochemically induced eliminations of benzene from the benzenethiolato osmium carbonyl cluster compound $HOs_3(CO)_{10}(\mu\text{-SPh})$ (**1**) have proved to be important routes for the synthesis of a variety of interesting new sulfido osmium carbonyl cluster compounds.[1-4] Perhaps the most intriguing of these compounds is the electron-rich cluster $Os_4(CO)_{12}(\mu_3\text{-S})_2$ (**2**), which readily and reversibly adds 1 mol of CO under mild conditions to form the open planar cluster $Os_4(CO)_{13}(\mu_3\text{-S})_2$. Recently, a mixed-metal analogue of **2**, $Os_3W(CO)_{12}(PMe_2Ph)(\mu_3\text{-S})_2$, has been made, and it exhibits bonding and reactivity properties similar to those of **2**.[5]

†Permanent address: Department of Chemistry, University of South Carolina, Columbia, SC 29208

(1) Adams, R. D.; Yang, L. W. *J. Am. Chem. Soc.* **1982**, *104*, 4115.
(2) Adams, R. D.; Yang, L. W. *J. Am. Chem. Soc.* **1983**, *105*, 235.
(3) Adams, R. D.; Horváth, I. T., Segmuller, B. E.; Yang, L. W. *Organometallics* **1983**, *2*, 1301.
(4) Adams, R. D.; Horváth, I.T.; Kim, H. S. *Organometallics* **1984**, *3*, 548.

0020-1669/84/1323-4718$01.50/0